Fluid Dynamics and Co-located Conferences
June 24-27, 2013, San Diego, CA
44th AIAA Thermophysics Conference

Modeling of Strong Nonequilibrium in Nitrogen Shock Waves

Jae Gang Kim* and Iain D. Boyd†
University of Michigan, Ann Arbor, MI 48109, USA

One dimensional post-normal shock flow calculations are carried out using state-of-the-art thermochemical nonequilibrium models. Two-temperature, four-temperature, and electronic master equation coupling models are adopted in the present work. In the four-temperature model, the rotational nonequilibrium is described by Parker and modified Park models. In the electronic master equation coupling model, recently evaluated electron and heavy-particle impacts and radiative transition cross sections are employed in constructing the system of electronic master equations. In analyzing the shock-tube experiments, the results calculated by the state-of-the-art thermochemical nonequilibrium models are compared with existing shock-tube experimental data. The four-temperature and electronic master equation coupling models with rotational nonequilibrium described by the modified Park model approximately reproduce the measured rotational, vibrational, and electronic temperatures.

I. Introduction

THE energy modes contained in atoms or molecules are usually characterized by a temperature. In a thermochemical nonequilibrium gas mixture, the temperatures which characterize these different modes of energy may be different from each other. Two-temperature and multi-temperature models[1] are widely used approaches for characterizing these different energy modes. In the two-temperature model, one approximates this situation with two main assumptions. First, one assumes that there are only two different temperatures. The rotational temperature of molecules is assumed to be the same as the translational temperature of heavy particles. Vibrational temperatures of all molecules are assumed to be the same as the electron temperature and the electronic temperature. Second, the forward and reverse rate coefficients for the chemical reactions involving molecules are assumed to be a function of a geometrically averaged temperature evaluated using the translational and vibrational temperatures. In the multi-temperature approach, unlike the two-temperature model, the vibrational temperature is considered as a species dependent characteristic temperature. Computational fluid dynamic results calculated by these temperature models show fairly good agreement with previous flight experiments.[2] However, the two-temperature and multi-temperature models are not able to correctly predict the shock stand-off distance for a sphere at intermediate hypersonic speeds between Mach numbers of 10 to 15 in air. In the work of Furudate et al.,[3] a comparison of the measured and calculated shock stand-off distances was performed. The measurement was made in a ballistic range in Tohoku University. The calculations were made using the extended two-temperature model in which the vibrational temperatures of O_2, N_2, and NO were considered different from each other. In this work, it was shown that the two-temperature model tends to underestimate the shock stand-off distance. In reentry calculations where the velocity exceeds 10km/sec, significant diffierences are shown between the results calculated by those thermochemical models and measured data.[4] These disagreements between the calculated and measured data show the uncertanties of two- and multi-temperature models and also show that the thermochemical nonequilibrium behind a strong shock wave is not understood well in the intermediate and higher hypersonic speeds.

One of the modeling uncertainties is the rotational nonequilibrium of air species. The spectrum of radiation emitted in the flow behind a shock wave was measured and analyzed by several researchers.[5,6]

*Post-doctoral Research Fellow, Department of Aerospace Engineering, 1320 Beal Avenue, Member of AIAA.
†Professor, Department of Aerospace Engineering, 1320 Beal Avenue, AIAA Fellow.

At the point of peak radiation intensity of the $N_2(2+)$ band, the spectrum was analyzed in detail. From such analyses, it was found that the rotational temperature is not higher than the vibrational temperature at the peak-intensity point. In a recent measurement by the Coherent Anti-Stokes Raman Spectroscopy (CARS) method,[7] the temperature of electronic ground state N_2 was estimated from radiation of the strong shock wave in a free-piston, double-diaphragm shock tube. In this experiment, the estimated rotational temperature is not higher than the vibrational temperature. In the theoretical calculations of electronic ground state N_2, master equation studies and 1-D post-normal shock flow calculations were performed by Kim and Boyd[8] by using a NASA database[9,10] of state-to-state transition rates for N_2. In this study, it was recommended that the rotational energy N_2 should be treated as a nonequilibrium mode in hypersonic reentry calculations.

In the present work, 1-D post-normal shock flow calculations of N_2 are carried out to analyze existing shock-tube experiments[5–7] by state-of-the-art thermochemical nonequilibrium models. The two-temperature (2-T), four-temperature (4-T), and electronic master equation coupling (EM) models are adopted in these post-normal shock flow analyses. In the 4-T model, the rotational, vibrational, and electron-electronic energies are considered as nonequilibrium modes. The rotational nonequilibrium of the 4-T model is described by Parker[11] and modified Park models[8,12] in the present work. In the EM model, the nonequilibrium populations of the electronic states of N and N_2 are determined by solving the system of electronic master equations in order to treat the electronic nonequilibrium energy mode. The system of electronic master equations is constructed by recently evaluated electron and heavy particle impacts and radiative transition cross sections of N and N_2. This system of electronic master equations is coupled with the 4-T model with the rotational nonequilibrium of modified Park model in calculating the post-normal shock flows.

II. Thermochemical nonequilibrium model

In the present work, 5 species of N, N_2, N^+, N_2^+, and e^- are adopted to carry out the post-normal shock flow calculations. In the neutral species, 82 electronic states of N and 5 electronic states of N_2 are employed, and in charged species, the electronic ground states of N^+ and N_2^+ are considered. The spectral data of each electronic states are obtained from SPRADIAN07 database.[13]

In calculating the post-normal shock flows, the jump conditions immediately behind a shock wave are derived by using the Rankine-Hugoniot relations assuming the electronic, rotational, and vibrational energy modes to be frozen. The downstream flow is calculated by solving one-dimensional conservation equations of mass, momentum, and global energy. These conservation equations are defined as

$$\frac{\partial}{\partial x}\begin{bmatrix} \rho_s u \\ \rho u^2 + p \\ \rho u\left(h + \frac{1}{2}u^2\right) \end{bmatrix} = \begin{bmatrix} m_s \omega_s \\ 0 \\ -Q_{rad} \end{bmatrix}, \tag{1}$$

where s is species index, ρ is density, x and u are the distance from the shock wave and the downstream velocity, respectively. h is specific enthalpy, m_s is species mass, and ω_s is the rate of species number density. In the 2-T and 4-T models, the radiative energy loss Q_{rad} is set to zero. However, in the EM model, the radiative energy loss caused by the radiative processes is considered in the global energy conservation equation. In addition to Eq. (1), the thermochemical nonequilibrium equations of the 2-T, 4-T, and EM models are solved to analyze the 1-D post-normal shock flows.

A. Two-temperature model

In the 2-T model, the electron-translational energy (e-T), electron-rotational energy (e-R), vibrational-translational energy (V-T) transfers, and energy removal due to chemical reactions are adopted in describing the relaxation of electron-electronic-vibrational energy. Then, the electron-electronic-vibrational energy

conservation equation is constructed as

$$
\begin{aligned}
u\frac{\partial E_{eev}}{\partial x} &= \sum_{s}^{h} N_a\gamma_e\frac{2m_e}{m_s}v_s\frac{3}{2}k(T-T_{eev}) + \sum_{s}^{m} N_a\gamma_e\frac{2m_e}{m_s}g_{r,s}v_s\frac{3}{2}k(T-T_{eev}) \\
&+ \sum_{s}^{m}\left[f_D\frac{\widetilde{e_{v,s}}(T)N_a\gamma_s - E_{v,s}}{\tau_{v,s}}\right] \\
&- \Psi_v D_{N_2}N_a\omega_{D_h} - D_{N_2}N_a\omega_{D_e} - I_N N_a\omega_{EI} \\
&+ \Psi_v D_{N_2^+}N_a\omega_{AI} - \Psi_v(D_{N_2} - D_{N_2^+})N_a\omega_{CER},
\end{aligned}
\tag{2}
$$

where N_a is Avogadro's number, γ is species concentration, and k is the Boltzmann constant. In the energy loss term of Eq. (2), D and I are the dissociation and ionization energies, respectively. In Eq. (2), ω_D are the dissociation rates by the electron and heavy particle impact processes, ω_{EI} is the electron impact ionization rate, ω_{AI} is the associative ionization rate, and ω_{CER} is the charge exchange reaction rate. In the 2-T model, all of the chemical reactions are treated by Arrhenius-type rate coefficients with geometrically averaged temperature of the translational and electron-electronic-vibrational temperatures of T and T_{eev}. In the present work, the reaction rate parameters are obtained from the reference data proposed by Park et al.[14] In evaluating the backward chemical reactions, the equilibrium constants are applied to derive the backward reaction rates, and these equilibrium constants are calculated by rigorous method of partition function relations.[1] In the present work, the normalized vibrational energy loss ratio Ψ_v is set to a constant of 0.5. From recent master equation studies[8,15] of N_2 and H_2, the energy loss ratio approaches a value of 0.5 in the vibrational mode. In the e-T transfer of Eq. (2), the collision frequency v_s is calculated by the following equation as

$$
v_s = n_s\sigma_{e,s}\left(\frac{8kT_{eev}}{\pi m_e}\right)^{1/2}, \tag{3}
$$

where n_s is species number density and m_e is electron mass. In the present work, the effective cross section $\sigma_{e,s}$ for neutral species is obtained from a curve-fit value proposed by Gnoffo et al.[16] For charged species, the effective cross section with the Debye cut-off approximation[1] is adopted in the present work;

$$
\sigma_{e,s} = \frac{4}{3}\frac{4.39\times10^{-6}}{T_{eev}^2}ln\left(\frac{1.24\times10^4 T_{eev}^{1.5}}{\sqrt{n_e}}\right), \tag{4}
$$

where n_e is the electron number density. In the e-R transfer of Eq. (2), a model proposed by Nishida and Matsumto[17] is employed. In the present work, the coefficient $g_{r,s}$ of the e-R transfer is set to a constant of 10.0 for neutral and charged particles. In the V-T transfer, the Millikan-White relaxation time[18] $\tau_{v,s}$ with the collision-limited correction term[19] τ_c is adopted in the present work. This collision-limited correction term is defined as

$$
\tau_c = \left(n_t\sigma_v\sqrt{\frac{8kT}{\pi\mu}}\right)^{-1}, \tag{5}
$$

$$
\sigma_v = {\sigma_v}^*\left(\frac{50,000}{T}\right)^2, \tag{6}
$$

where n_t and μ are the total number density of colliding particles and the average mass of the mixture, respectively. In the 2-T model, σ_v^* is set to $3.0\times10^{-17}\ cm^2$ as proposed by Park.[19] The diffusion correction factor f_D of the V-T transfer in Eq. (2) is defined as

$$
f_D = \left|\frac{T_s - T_{eev}}{T_s - T_{eev,s}}\right|^{a-1}, \tag{7}
$$

where a is an arbitrary parameter given as $3.5\times exp(-5,000/T_s)$ for N_2 and N_2^+. T_s and T_{vs} are the translational and electron-electronic vibrational temperatures immediately behind the shock wave.

B. 4-Temperature model

In the 4-T model, four pools of energy are considered consisting of the translational, rotational, vibrational, and electron-electronic energy modes. In describing rotational nonequilibrium, Parker[11] and modified Park[8,12] models are taken into account in the present work.

In the Parker model, rotational-translational energy (R-T) transfer is treated by a Landau-Teller type of equation with the theoretically calculated R-T relaxation time. This relaxation time was derived by using the rigid rotator assumption.[11] Then, the rotational energy conservation equation is constructed by the e-R and R-T transfers and the rotational energy losses due to chemical reactions;

$$\begin{aligned} u\frac{dE_r}{dx} = &-\sum_s^m N_a\gamma_e\frac{2m_e}{m_s}g_{r,s}v_s\frac{3}{2}k(T_r-T_{ee}) + \sum_s^m\left[\frac{\widetilde{e_{r,s}}(T)N_a\gamma_s - E_{r,s}}{\tau_{r,s}}\right] \\ &- \Psi_r D_{N_2}N_a\omega_D + \Psi_r D_{N_2^+}N_a\omega_{AI} - \Psi_r(D_{N_2}-D_{N_2^+})N_a\omega_{CER}, \end{aligned} \tag{8}$$

where T_r and T_{ee} are the rotational and electron-electronic temperatures, respectively. The normalized rotational energy loss ratio Ψ_r is set to a constant of 0.3 in the present work. The R-T relaxation time $\tau_{r,s}$ of the Parker model is defined as

$$\tau_{r,s} = Z_{R,s}\left[\sum_k \sigma_{rot}n_k\left(\frac{8kT}{\pi\mu_{s,k}}\right)\right]^{-1}, \tag{9}$$

and $Z_{R,s}$ is given by

$$Z_{R,s} = \frac{Z_{R,s}^{\infty}}{1+\frac{\pi^{3/2}}{2}\left(\frac{\theta_{rot,s}}{T}\right)^{1/2}+\left(\frac{\pi^2}{4}+\pi\right)\left(\frac{\theta_{rot,s}}{T}\right)}, \tag{10}$$

where $\theta_{rot,s}$ is the characteristic rotational temperature. In the present work, collision cross section σ_{rot} and number $Z_{R,s}^{\infty}$ are set to 10^{-15} cm^2 and 15.7 for N_2 and N_2^+, respectively. In the vibrational energy conservation equation, the electron-vibrational energy (e-V) and V-T transfers and the vibrational energy losses due to chemical reactions are adopted. This vibrational conservation equation is defined as

$$\begin{aligned} u\frac{\partial E_v}{\partial x} = &\frac{\widetilde{e_{v,N_2}}(T_{ee})N_a\gamma_s - E_{v,N_2}}{\tau_{eV_{N_2}}} + \sum_s^m\left[f_D\frac{\widetilde{e_{v,s}}(T)N_a\gamma_s - E_{v,s}}{\tau_{v,s}}\right] \\ &- \Psi_v D_{N_2}N_a\omega_D + \Psi_v D_{N_2^+}N_a\omega_{AI} - \Psi_v(D_{N_2}-D_{N_2^+})N_a\omega_{CER}, \end{aligned} \tag{11}$$

where e-V relaxation time τ_{eV} of N_2 is obtained from the measured value by Lee[20] with the curve fit function of electron-electronic temperature T_{ee}.

In the modified Park model,[8,12] the R-T relaxation time of N_2+N_2 proposed by Park[12] is adopted in the present work. This relaxation time was derived from the results of master equation calculations with the existing state-to-state rotational transition rates. This R-T relaxation time is much slower than the relaxation time proposed by Parker[11] at temperatures above 10,000 K. In rotational-vibrational energy (R-V) transfer of N_2+N_2, Kim and Boyd model[8] is adopted in the present work. In original Park's model[12] of the R-V transfer, the fractional contribution of the R-V to the total energy transfer is set to a constant of 0.4 and this value is derived from $f_{RV} = kT/(kT+1.5kT)$. In the present work, unlike Park's original model, the fractional contribution for species s is determined by

$$f_{RV,s} = \frac{(\xi_{v,s}/2)kT}{(\xi_{r,s}/2)kT+1.5kT}, \tag{12}$$

where $\xi_{r,s}$ and $\xi_{v,s}$ are the number of degrees of freedom of the rotational and vibrational modes, respectively. In the modified Park model, the rotational-vibrational-translational energy (R-V-T) transfer of $N_2(X^1\sum_g^+)$+$N(^4S)$ is calculated by coupling the full master equations[8] with the rovibrational state-to-state transition rates obtained from the NASA Ames database.[9,10] Then, the e-R, e-V, R-T, V-T, R-V, and R-V-T transfers and energy losses due to chemical reactions are employed in constructing the rotational and

vibrational energy conservation equations, and these are given as

$$
\begin{aligned}
u\frac{dE_r}{dx} =& -\sum_s^m N_a\gamma_e\frac{2m_e}{m_s}g_{r,s}v_s\frac{3}{2}k(T_r-T_{ee}) \\
&+\sum_s^m\left[\frac{\widetilde{e_{r,s}}(T)N_a\gamma_s-E_{r,s}}{\tau_{r,s}}+f_{RV,s}\frac{E_{v,s}-\widetilde{e_{v,s}}(T_r)N_a\gamma_s}{\tau_{v,s}}\right] \\
&+\sum_{i=N_2(X,v,J)}^{N_2(X)}\sum_{j=N_2(X,v,J)}^{N_2(X)}e_{r_{N_2}}(i)K(i,j)\left[\frac{Q_i}{Q_j}\gamma_j-\gamma_i\right]\rho N_a^2\gamma_{N(^4S)} \\
&-\sum_{i=N_2(X,v,J)}^{N_2(X)}e_{r_{N_2}}(i)K(i,c)\left[\gamma_i-\frac{Q_iQ_{t_{N_2}}}{Q_N^2Q_{t_N}^2}exp\left(\frac{D_i}{kT}\right)\rho N_a\gamma_{N(^4S)}^2\right]\rho N_a^2\gamma_{N(^4S)} \\
&-\sum_{i=N_2(X,v,J)}^{N_2(X)}e_{r_{N_2}}(i)K_p(i,c)\left[\gamma_i-\frac{Q_iQ_{t_{N_2}}}{Q_N^2Q_{t_N}^2}exp\left(\frac{D_i}{kT}\right)\rho N_a\gamma_{N(^4S)}^2\right]N_a \\
&-\Psi_rD_{N_2}N_a\omega_D+\Psi_rD_{N_2^+}N_a\omega_{AI}-\Psi_r(D_{N_2}-D_{N_2^+})N_a\omega_{CER},
\end{aligned}
\tag{13}
$$

$$
\begin{aligned}
u\frac{dE_v}{dx} =& \frac{\widetilde{e_{v,N_2}}(T_{ee})N_a\gamma_s-E_{v,N_2}}{\tau_{eV,N_2}} \\
&+\sum_s^m\left[(1-f_{RV,s})f_D\frac{\widetilde{e_{v,s}}(T)N_a\gamma_s-E_{v,s}}{\tau_{v,s}}+f_{RV,s}\frac{\widetilde{e_{v,s}}(T_r)N_a\gamma_s-E_{v,s}}{\tau_{v,s}}\right] \\
&+\sum_{i=N_2(X,v,J)}^{N_2(X)}\sum_{j=N_2(X,v,J)}^{N_2(X)}e_{v_{N_2(X)}}(i)K(i,j)\left[\frac{Q_i}{Q_j}\gamma_j-\gamma_i\right]\rho N_a^2\gamma_{N(^4S)} \\
&-\sum_{i=N_2(X,v,J)}^{N_2(X)}e_{v_{N_2(X)}}(i)K(i,c)\left[\gamma_i-\frac{Q_iQ_{t_{N_2}}}{Q_N^2Q_{t_N}^2}exp\left(\frac{D_i}{kT}\right)\rho N_a\gamma_{N(^4S)}^2\right]\rho N_a^2\gamma_{N(^4S)} \\
&-\sum_{i=N_2(X,v,J)}^{N_2(X)}e_{v_{N_2(X)}}(i)K_p(i,c)\left[\gamma_i-\frac{Q_iQ_{t_{N_2}}}{Q_N^2Q_{t_N}^2}exp\left(\frac{D_i}{kT}\right)\rho N_a\gamma_{N(^4S)}^2\right]N_a \\
&-\Psi_vD_{N_2}N_a\omega_D+\Psi_vD_{N_2^+}N_a\omega_{AI}-\Psi_v(D_{N_2}-D_{N_2^+})N_a\omega_{CER},
\end{aligned}
\tag{14}
$$

where indices of i and j denote the rovibrational state of $N_2(X)$, and $K(i,j)$ and $K(i,c)$ are the rovibrational state-to-state transition rates for $N_2(X)+N(^4S)$. In the modified Park model, the predissociation of $N_2(X)$ is included, and its rate is described by $K_p(i,c)$. In the previous master equation studies for $N+N_2$[8] and H_2,[15] it was observed that the rotational and vibrational relaxation times become identical when the temperature increases. In the work by Kim and Boyd,[8] the collision limiting cross section σ_v of Eq. (6) was modified to a constant of $3.0\times10^{-18}\ cm^2$ to satisfy these relaxation patterns. In the modified Park model, this corrected collision limiting cross section is employed. In species conservation equations of the modified Park model, all of the chemical reactions are described by using the Arrhenius type of equations except the dissociation of $N_2(X)+N(^4S)$ and the predissociation of $N_2(X)$. This dissociation and predissociation are evaluated by coupling the rovibrational master equation of the bound-free transitions. These are given as

$$
\omega_D|_{N_2+N}=\sum_{i=N_2(X,v,J)}^{N_2(X)}K(i,c)\left[\gamma_i-\frac{Q_iQ_{t_{N_2}}}{Q_N^2Q_{t_N}^2}exp\left(\frac{D_i}{kT}\right)\rho N_a\gamma_{N(^4S)}^2\right]\rho N_a\gamma_{N(^4S)}, \tag{15}
$$

$$
\omega_D|_{N_2}=\sum_{i=N_2(X,v,J)}^{N_2(X)}K_p(i,c)\left[\gamma_i-\frac{Q_iQ_{t_{N_2}}}{Q_N^2Q_{t_N}^2}exp\left(\frac{D_i}{kT}\right)\rho N_a\gamma_{N(^4S)}^2\right]. \tag{16}
$$

The electron-electronic energy conservation equation using the Parker and modified Park models is constructed by e-T, e-R, and e-V transfers and it defined as

$$u\frac{dE_{ee}}{dx} = \sum_{s}^{h} N_a\gamma_e\frac{2m_e}{m_s}v_s\frac{3}{2}k(T-T_{ee}) + \sum_{s}^{m} N_a\gamma_e\frac{2m_e}{m_s}g_{r,s}v_s\frac{3}{2}k(T_r-T_{ee}) - \frac{\widetilde{e_{v,N_2}}(T_{ee})N_a\gamma_s - E_{v,N_2}}{\tau_{eV,N_2}} - (1-\Psi_r-\Psi_v)D_{N_2}N_a\omega_{D_e} - I_N N_a\omega_{EI}. \quad (17)$$

C. Electronic master equation coupling model

In the EM model, the rotational and vibrational energy relaxations are treated in a similar way as the 4-T with the rotational nonequilibrium of the modified Park model. However, the number density populations of electronic states of N and N_2 are evaluated by solving the system of electronic master equations.

In atomic elementary processes of the system of electronic master equations, the N atom is more efficiently excited and ionized by electron impact than the heavy particle impact processes. In electron impact excitation, the excitation rates of the first three states of N are obtained from the work by Bultel et al.[21] The electronic state-to-state transition rates of the other states are obtained from the work by Panesi et al.[22] In electron impact ionization, the rate is well known for atomic hydrogen,[13] and this rate form is adopted for ionization of N in the present work. This electron impact ionization rate is defined as

$$K_e(i,c) = \frac{5.45}{T_e^{3/2}}\left[0.62\frac{kT_e}{I_N-E_i}E_1\left(\frac{I_N-E_i}{kT_e}\right) - 0.534\frac{E_1(E_c)}{E_c}\right], \quad (18)$$

where index i denotes the electronic state of N, and T_e is the electron temperature. E_c is $E_c = (I_N - E_i)/(kT_e) + 0.56$, and $E_1(\theta)$ is the exponential integration defined as

$$E_1(\theta) = \int_0^1 exp(-\theta/s)s^{-1}ds. \quad (19)$$

In molecular elementary processes, electron and heavy-particle impact excitation and dissociations are adopted in the EM model. The overall rate of electron impact excitation is defined as

$$\overline{K}_e(e,e') = \frac{\sum_v exp\left(-\frac{G_v}{kT_v}\right)\sum_J(2J+1)exp\left(-\frac{F_J}{kT_r}\right)\sum_{v'}q(v,v')\sum_{J'}(2J'+1)K(e,v,J;e',v',J')}{\sum_v exp\left(-\frac{G_v}{kT_v}\right)\sum_J(2J+1)exp\left(-\frac{F_J}{kT_r}\right)}, \quad (20)$$

where $q(v,v')$ is the Frank-Condon factor. G_v and F_J are the vibrational and rotational energies, respectively. In Eq. (20), the rate of transition $K_e(e,v,J;e',v',J')$ is given by

$$K(e,v,J;e',v',J') = \frac{8\pi}{\sqrt{m_e}}\left(\frac{1}{2\pi kT_e}\right)^{3/2}\int_{E*}^{\infty}\sigma_e exp\left(-\frac{E}{kT_e}\right)EdE, \quad (21)$$

where E^* is a threshold energy for electronic excitation, and σ_e is the electron impact excitation cross section. In the present work, the electron impact excitation cross section and Frank-Condon factor are obtained from the SPRADIAN07 database.[13] In the EM model, the electron impact dissociation of the molecular elementary processes is given by

$$K_e^D(i,c) = A\left(\frac{T_e}{6,000}\right)^n exp\left(-\frac{T_d}{T_e}\right), \quad (22)$$

where the parameters A, n, and T_d are obtained from a database of electron-impact transition rates proposed by Park.[23] In the heavy-particle impact excitation and dissociation, the bound-bound and bound-free transition rates are given as

$$K_h(i,j) = A\left(\frac{T}{6,000}\right)^n exp\left(-\frac{T_d}{T}\right), \quad (23)$$

where the parameters A, n, and T_d are obtained from a database of heavy particle impact transition rates proposed by Park.[24]

In radiative transition processes, the radiative transition model for N is obtained by grouping elementary levels having similar characteristics. The equivalent spontaneous emission probability of each average level is determined based on the detailed emission probabilities of the SPRADIAN07 database.[13] In the present work, radiative and dielectric recombination is adopted in describing the recombination of N^+ and e^-, and the rate coefficients are obtained from the work by Bourdon and Vervisch.[25] In the radiative transitions for N_2, the radiative transition probability from the electronic state i to state $j < i$ is expressed as

$$A(i,j) = \frac{\sum_v A_v(i,j) exp\left(-\frac{G_v}{kT_v}\right)}{\sum_v exp\left(-\frac{G_v}{kT_v}\right)}, \tag{24}$$

where the transition probabilities $A_v(i,j)$ are obtained from the SPRADIAN07 database.[13] In the present work, the possible reabsorption of the emitted radiation is estimated by using the escape factors α without solving the radiative transport equations. It is assumed that an optically thin medium is associated with an escape factor of one, whereas for an optically thick medium, the escape factor is set to zero.

The system of electronic master equation of N and N_2 can be constructed by the electron and heavy particle impact and radiative transitions, and the rates of the electronic concentration of N can be written as

$$\begin{aligned}
u\frac{\partial \gamma_i}{\partial x} &= \sum_j^N K_e(i,j)\rho N_a \gamma_e \left[\frac{Q_i^e}{Q_j^e}\gamma_j - \gamma_i\right] \\
&+ K_e(i,c)\rho N_a \gamma_e \left[\frac{Q_i^e Q_{t_N}^e}{Q_{N^+}^e Q_{t_{N^+}}^e Q_e Q_{t_e}^e} exp\left(\frac{I_N}{kT_e}\right)\rho N_a \gamma_{N^+}\gamma_e - \gamma_i\right] \\
&- \sum_j^{N_2} \delta_{i,k}\epsilon_{k,l} K_e^D(j,c)\rho N_a \gamma_e \left[\frac{Q_j^e Q_{t_{N_2}}^e}{Q_{N(k)}^e Q_{N(l)}^e (Q_{t_N}^e)^2} exp\left(\frac{D_j}{kT_e}\right)\rho N_a \gamma_{N(k)}\gamma_{N(l)} - \gamma_{N_2(j)}\right] \\
&- \sum_j^{N_2}\sum_s^h \delta_{i,k}\epsilon_{k,l} K_{h,s}^D(j,c)\rho N_a \gamma_s \left[\frac{Q_j^h Q_{t_{N_2}}^h}{Q_{N(k)}^h Q_{N(l)}^h (Q_{t_N}^h)^2} exp\left(\frac{D_j}{kT}\right)\rho N_a \gamma_{N(k)}\gamma_{N(l)} - \gamma_{N_2(j)}\right] \\
&- 2\delta_{i,1} \sum_{j=N_2(X,v,J)}^{N_2(X)} K_{(j,c)}^{N_2(X)+N(^4S)} \left[\frac{Q_j^h Q_{t_{N_2}}^h}{(Q_{N(^4S)}^h Q_{t_N}^h)^2} exp\left(\frac{D_j}{kT}\right)\rho N_a \gamma_{N(^4S)}^2 - \gamma_j\right]\rho N_a \gamma_{N(^4S)} \\
&- 2\delta_{i,1} \sum_{j=N_2(X,v,J)}^{N_2(X)} K_p^{N_2(X)}(j,c) \left[\frac{Q_j^h Q_{t_{N_2}}^h}{(Q_{N(^4S)}^h Q_{t_N}^h)^2} exp\left(\frac{D_j}{kT}\right)\rho N_a \gamma_{N(^4S)}^2 - \gamma_j\right] \\
&+ \sum_{j,j>i}^N \alpha_{j,i} A(j,i)\gamma_j - \sum_{j,j<i}^N \alpha_{i,j} A(i,j)\gamma_i + \left[\alpha_i^{RR} K_{RR}(c,i) + \alpha_i^{DR} K_{DR}(c,i)\right]\rho N_a \gamma_{N^+}\gamma_e,
\end{aligned} \tag{25}$$

where k and l denote the electronic states of dissociated N atom. δ is the Dirac delta function, ϵ is the symmetric factor defined as $\epsilon_{k,l} = 2$ if $k = l$ or $\epsilon_{k,l} = 1$ if $k \neq l$. K_e is the electronic impact excitation rate. K_e^D and K_h^D are the electron and heavy-particle impact dissociation rates. K_{RR} and K_{DR} are the radiative and dielectric recombination rates, respectively. In Eq. (25), Q^e is the partition function defined by the electron temperature T_e, and Q^h is defined by the translational temperature T. The rates of the electronic

concentration of N_2 is expressed as

$$
\begin{aligned}
u\frac{\partial \gamma_i}{\partial x} &= \sum_{j}^{N_2} K_e(i,j)\rho N_a \gamma_e \left[\frac{Q_i^e}{Q_j^e}\gamma_j - \gamma_i\right] \\
&+ K_e^D(i,c)\rho N_a \gamma_e \left[\frac{Q_i^e Q_{t_{N_2}}^e}{Q_{N(k)}^e Q_{N(l)}^e (Q_{t_N}^e)^2} exp\left(\frac{D_i}{kT_e}\right)\rho N_a \gamma_{N(k)}\gamma_{N(l)} - \gamma_i\right] \\
&+ \sum_{s}^{h}\sum_{j}^{N_2} K_{h,s}(i,j)\rho N_a \gamma_s \left[\frac{Q_i^h}{Q_j^h}\gamma_j - \gamma_i\right] \\
&+ \sum_{s}^{h} K_{h,s}^D(i,c)\rho N_a \gamma_s \left[\frac{Q_i^h Q_{t_{N_2}}^h}{Q_{N(k)}^h Q_{N(l)}^h (Q_{t_N}^h)^2} exp\left(\frac{D_i}{kT}\right)\rho N_a \gamma_{N(k)}\gamma_{N(l)} - \gamma_i\right] \\
&+ \delta_{i,1} \sum_{j=(v,J)}^{N_2(X)} K_{(j,c)}^{N_2(X)+N(^4S)} \left[\frac{Q_j^h Q_{t_{N_2}}^h}{(Q_{N(^4S)}^h Q_{t_N}^h)^2} exp\left(\frac{D_j}{kT}\right)\rho N_a \gamma_{N(^4S)}^2 - \gamma_j\right]\rho N_a \gamma_{N(^4S)} \\
&+ \delta_{i,1} \sum_{j=(v,J)}^{N_2(X)} K_p^{N_2(X)}(j,c) \left[\frac{Q_j^h Q_{t_{N_2}}^h}{(Q_{N(^4S)}^h Q_{t_N}^h)^2} exp\left(\frac{D_j}{kT}\right)\rho N_a \gamma_{N(^4S)}^2 - \gamma_j\right] \\
&+ \sum_{j,j>i}^{N_2} \alpha_{j,i} A_{N_2}(j,i)\gamma_j - \sum_{j,j<i}^{N_2} \alpha_{i,j} A_{N_2}(i,j)\gamma_i.
\end{aligned}
\tag{26}
$$

In the EM model, the electron energy loss and gain due to electron impact processes of the bound-bound and bound-free transitions need to be considered. In the present work, these detailed electron energy loss and gain are fully implemented in the electron energy conservation equation of Eq. (17) with some modifications. Also, in the EM model, the rotational and vibrational energy loss and gain due to chemical reactions of Eqs. (13) and (14) are modified to describe the chemical reactions in each electronic state. In the EM model, the associative ionization and charge exchange reaction are considered by the Arrhenius type of equations with an assumption that these reactions occur in the electronic ground state. The radiative energy loss Q_{rad} due to radiative transition and radiative recombination of Eq.(1) is modeled as

$$
\begin{aligned}
Q_{rad} &= \sum_{s}^{N,N_2} \sum_{i,j,j<i} \alpha_{i,j}(E_i - E_j) A_s(i,j) N_a \gamma_i \\
&+ \sum_{i}^{N} (I_N - E_i)\left[\alpha_i^{RR} K_{RR}(c,i) + \alpha_i^{DR} K_{DR}(c,i)\right]\rho N_a^2 \gamma_{N^+}\gamma_e.
\end{aligned}
\tag{27}
$$

III. Post-normal shock flow calculations

The post-normal shock flow calculations are carried out for existing shock-tube experiments[5–7] by the state-of-the-art thermochemical nonequilibrium 2-T, 4-T, and EM models. The results from the calculations are compared with the shock-tube measured data and analyzed in detail. In the present work, the post-normal shock flow calculations are performed by the implicit integration method with parallelization algorithm to speed up the computation time.

In Fig. 1, the calculated translational, rotational, and vibrational temperatures by the 2-T, 4-T, and EM models are compared with the shock-tube data measured by Sharma and Gillespie[5] and AVCO.[26] In these calculations, the upstream pressure is 1.0 $Torr$ and the shock velocity is 6.2 km/sec. In this case, the total enthalpy of the free-stream is about 20 MJ/kg and the density is 1.497×10^{-6} g/cm^3. In figure (a), the calculated results by the 2-T and 4-T with Parker models are compared with the experimental values. The rotational and vibrational relaxations between the 2-T and 4-T models are almost identical, and the rotational relaxation of the 4-T model is fast enough to treat as an equilibrium temperature. In comparison with the experimental values, it is shown that the relaxations of the rotational and vibrational temperatures are much faster than the measured value by Sharma and Gillespie, and the rotational temperature underestimates the measured rotational temperature by AVCO. In figure (b), the calculated temperatures by the 4-T with

modified Park and EM models are compared with the shock-tube measured values. The calculated rotational relaxation of the 4-T with modified Park model is slow enough to treat as a nonequilibrium state, and the calculated rotational and vibrational temperatures agree with the data measured by Sharma and Gillespie. In the downstream, the rotational temperature of the EM model is slightly lower than the 4-T with modified Park model. However, the calculated rotational temperature of the 4-T with modified Park and EM models agree with the data measured by AVCO.

In Fig. 2, the calculated electronic temperature of $N_2(B^3\Pi_g)$ by the 2-T, 4-T, and EM models are compared with the shock-tube data measured by AVCO.[26] In the EM model, the electronic excitations with and without heavy-particle impact processes are also compared. In the 2-T and 4-T with Parker model, the estimated electronic temperatures of T_{eev} and T_{eex} are higher than the measured electronic temperature of $N_2(B^3\Pi_g)$ by AVCO. In the 4-T with modified Park model, the estimated electronic temperature of T_{eex} is also higher than the measured value, and it cannot accurately reproduce the electronic temperature of $N_2(B^3\Pi_g)$ immediately behind the shock wave. However, in comparisons of the electronic temperature between the EM model and the experimental values, the calculated electronic temperature of $N_2(B^3\Pi_g)$ with the heavy-particle impact processes agrees with the measured values immediately behind the shock wave and also further downstream. In the electronic temperature of the EM model without the heavy-particle impact processes, it is difficult to describe the electronic excitation immediately behind the shock wave. This is because the number density of electrons is not enough to excite the electronic energy levels of N_2 behind the shock wave, and most of the electronic excitation of N_2 occurs through the heavy-particle impact processes. After the electrons are generated by associative ionization, the electron impact processes become important in the electronic excitation of N_2.

In Fig. 3, the electronic nonequilibrium populations of N and N_2 of the EM model are compared with those of the Boltzmann distributions specified by the electron temperature. In figure (a), the nonequilibrium populations of N are presented. Immediately behind the shock wave, large deviations of the number density between the EM model and the Boltzmann distributions are observed in the highly excited states. The populations of the low electronic states can be treated as Boltzmann distributions specified by electron temperature. However, the nonequilibrium populations of the highly excited states are not converged to the Boltzmann distributions. This phenomenon is typical of the nonequilibrium conditions encountered during a high-speed shock velocity.[22] In figure (b), the number density populations of the electronic states of N_2 from the EM model is compared with the Boltzmann distributions. Weak deviations between the nonequilibrium populations and the Boltzmann distributions are observed behind the shock wave, and these nonequilibrium populations are almost converged to the Boltzmann distributions in the downstream.

In Fig. 4, the species mole-fractions of the 2-T, 4-T, and EM models are compared. In figures (a) and (b), it is observed that the chemical reactions by the 2-T and 4-T with Parker models occur more rapidly than the chemical reactions by the 4-T with modified Park and EM models. This is because, immediately behind the shock wave, the heavy particle impact dissociation has an important role in chemical reactions, and this dissociation is dominated by the rotational and vibrational relaxations. As seen in Fig. 1, such relaxations of the 2-T and 4-T with Parker models are much faster than those of the 4-T with modified Park and EM models. When the dissociated N atom is generated, the electron is easily produced by associative ionization. Then, the electron impact processes and the other chemical reactions occur. These results show that the heavy-particle impact rotational and vibrational relaxations immediately behind the shock wave have an important role in the nonequilibrium chemical reactions in post normal shock flows.

In Fig. 5, comparisons of the calculated translational, rotational, vibrational, and electronic temperatures with the shock-tube experiments by Sakurai et al.[7] are presented in an optically thin medium. In the shock-tube experiment, the CARS method was employed to measure the temperatures of the ground state from the radiation behind the strong shock wave. ND:YAG and dye lasers were used in this method. When these lasers excited the nitrogen molecules behind the shock wave, the CARS signal was collected by a spectrograph. Then, the rotational and vibrational temperatures were estimated using a spectral matching method. In this shock-tube experiment by CARS, the rotational and vibrational temperatures were measured at the shock wave velocity of 7.6 km/sec and ambient pressure of 2.5 $Torr$. In the present work, the post-normal shock flow calculations are performed for these conditions. In figure (a), it is observed that the calculated rotational and vibrational temperatures of the 4-T with modified Park and EM models increase more slowly behind the shock wave than those of the 2-T and 4-T with Parker models. Also, the rotational and vibrational relaxations are almost identical in the 4-T with modified Park and EM models. In comparing with the measured values, the rotational temperature of the 4-T with modified Park and EM models is almost the

same as the measured temperature. The vibrational temperature of the 4-T with modified Park and EM models is slightly higher than the measured value. However, there exists a discernable difference between the calculated rotational and vibrational temperatures of the 2-T and 4-T with Parker models and shock-tube measured values. In figure(b), the comparisons of the electronic temperature of N and N_2 are presented. The estimated electronic temperatures of the 2-T and 4-T with Parker models rapidly increase because of the e-T and e-V transfers of N_2. However, the electronic temperatures of the 4-T with modified Park and EM models slowly increase because the vibrational relaxation occurs more slowly than the 2-T and 4-T with Parker models. Also, in the EM model, it is shown that the heavy-particle impact processes efficiently affect the electronic excitation of N_2 behind the shock wave.

In Fig. 6, the nonequilibrium populations of N and N_2 of the EM model are compared with those of the Boltzmann distributions specified by the electron temperature. In figure (a), it is shown that the nonequilibrium populations of the low electronic energy of N are enough to treat as the Boltzmann distributions specified by electron temperature. However, the nonequilibrium populations of the highly excited states are not converged to the Boltzmann distributions. In figure (b), the number density populations of the EM model and the Boltzmann distributions are compared for the electronic states of N_2. Immediately behind a shock wave, weak deviations between the nonequilibrium populations and the Boltzmann distributions are observed, and the nonequilibrium populations are almost converged to the Boltzmann distributions specified by the electron temperature in the downstream.

In Fig. 7, comparisons of the species mole-fractions from the 2-T, 4-T, and EM models are presented. In figures (a) and (b), it is observed that the chemical reactions by the 2-T and 4-T with Parker models occur more rapidly than the chemical reactions by the 4-T with modified Park and EM models because the rotational and vibrational relaxations of the 2-T and 4-T with Parker models are much faster than the 4-T with modified Park and EM models. These rotational and vibrational relaxations affect the heavy-particle impact dissociations, and the other chemical reactions are triggered by the dissociated N atoms. In figure (b), the chemical reactions of the EM model occur more rapidly than those of the 4-T with modified Park model. In the EM model, the heavy-particle impact dissociation of each electronic state of N_2 is described, and these chemical reactions produce faster dissociation than the 4-T with the modified Park model. The fast dissociation affects the associative ionization, electron impact processes, and the other chemical reactions.

In Fig. 8, the computed translational, rotational, vibrational, and electronic temperatures are compared with the shock-tube experiments by Fujita et al.[6] In the shock-tube experiments, air radiation from behind strong shock waves was measured for the $N_2(2+)$ system using a free-piston double-diaphragm shock tube. The spatial variation of radiation spectra was obtained using spatially resolved imaging spectroscopy at a shock velocity of 11.9 km/sec in the ambient pressure at 0.3 $Torr$. A series of point wise spectroscopy analysis was carried out in order to obtain a spatial profile of temperatures. In the post-normal shock flow calculations, the freestream conditions are set to the shock-tube experimental conditions. In figures (a) to (c), the rotational relaxation of the 4-T with Parker model is more rapidly converged to the translational temperature than the vibrational temperature. In the comparisons of the rotational and vibrational temperatures between the 2-T and 4-T with Parker models and the experimental values, it is shown that the calculated vibrational temperatures overestimate the measured temperatures, and the calculated rotational temperature of the 4-T with Parker model has a discernable difference with the measured rotational values. In the rotational and vibrational temperatures of the 4-T with modified Park and EM models, the relaxations occur more slowly than those of the 2-T and 4-T with Parker models, and the calculated rotational and vibrational temperatures fall within the error bars of the measured rotational and vibrational temperatures. These results show that strong rotational and vibrational nonequilibrium exists behind the strong shock wave, and the 4-T with modified Park and EM models can capture this phenomenon. However, in figure (d), the electronic temperatures of the 4-T with modified Park and EM models do not accurately reproduce the measured electronic temperature of N. As shown in Figs. 2 and 5, the electronic excitation behind the shock wave is mostly affected by the heavy-particle impact processes. In Fujita's experiments, the translational temperature immediately behind the shock is about $90,000\ K$, and this temperature is beyond the available temperature range to describe the heavy-particle impact processes by the existing transition rate data. The existing heavy-particle impact transition rates were mostly extrapolated from rates at temperatures under $3,000\ K$. For this limitation, it is difficult to accurately reproduce the measured electronic temperature.

In Fig. 9, comparisons of the species mole-fractions from the 2-T, 4-T, and EM models are presented. In figures (a) and (b), it is shown that the chemical reactions by the 4-T with modified Park and EM models occur more slowly than those of the 2-T and 4-T with Parker models. These patterns of the chemical

reactions are observed in Figs. 4 and 7. Unlike the chemical reactions in the above post-normal shock flow cases, the electron impact ionization and radiative recombination are dominant chemical reactions in the downstream. In the EM model, such electron impact ionization and radiative recombination are accurately described by considering the chemical reactions of each electronic state. In figures (c) and (d), comparisons of the mole-fractions and the electron number density associated with the radiative escape factor are presented. Immediately behind the shock wave, the effect of the radiative escape factor is not obviously shown. However, in the downstream, the escape factor has an important role in the radiative and dielectric recombination. The electrons produced by electron impact ionization recombine by the radiative processes, and the electron number density in the optically thick medium is about two times larger than that in the optically thin medium.

IV. Conclusions

In the present work, 1-D post-normal shock flow calculations of N_2 are carried out in order to analyze the existing shock tube experiments by Sharma and Gillespie, Sakurai et al., and Fujita et al. The state-of-the-art thermochemical nonequilibrium models of the two-temperature (2-T), four-temperature (4-T), and electronic master equation coupling (EM) models are adopted in the present work. In the 4-T model, the rotational nonequilibrium is described by Parker and modified Park models. In the EM model, the system of electronic master equations is constructed by the recently evaluated electron and heavy-particle impacts and radiative transition cross sections. In the 4-T with modified Park and EM models, the rotational and vibrational relaxations are slow enough to be treated as a nonequilibrium state, and the calculated temperatures agree with the shock-tube measured data. However, the rotational relaxation of the 4-T with Parker model is much faster than the 4-T with modified Park and EM models. These rotational and vibrational relaxations affect the heavy-particle impact dissociation behind the shock wave. As a result of these relaxations, the chemical reactions of the 4-T with modified Park and EM models occur more slowly than the chemical reactions of the 2-T and 4-T with Parker models. Immediately behind the shock wave, the electronic states are mostly excited by the heavy-particle impact processes, and the measured electronic temperatures at the intermediate shock speed oft 6 km/sec are accurately reproduced by the present EM model. However, there is a limitation to describe the excitation at a translational temperature above $90,000\ K$ because this temperature is beyond the available range to describe heavy-particle impact processes by the existing transition rate data. In the chemical reactions of the high speed and high temperature flows, the electron impact ionization and radiative recombination are dominant chemical reactions in the downstream flows, and the radiative escape factor has an important role in describing these processes.

Acknowledgement

The authors thank Dr. R. Jaffe, and Dr. D. Schwenke at NASA Ames Research Center for providing the rovibrational state-to-state transition data of $N + N_2$. We also gratefully acknowledge Dr. C. Park and Dr. M. Panesi for useful discussion on the electron and heavy-particle impact excitation processes. The authors also gratefully acknowledge funding for this work through Air Force Office of Scientific Research Grants FA9550-11-1-0309 and FA9550-12-1-0483.

References

[1]Park, C., *Nonequilibrium Hypersonic Aerothermodynamics*, Wiley, New York, 1990.

[2]Gupta, R. N., Moss, J. N., and Price, J. M., "Assessment of Thermochemical Nonequilibrium and Slip Effects for Orbital Reentry Experiment(OREX)," NASA TM-111600, July 1996.

[3]Furudate, M., Nonaka, S., and Swada, K., Calculation of Shock Shapes over Simple Geometries in Intermediate Hypersonic Air Flow, AIAA 1999-3686, *33rd AIAA Thermophysics Conference and Exhibit*, Orlando, Florida, 1999.

[4]Suzuki, K., Kubota, H., Fujita, K., and Abe, T., "Chemical Nonequilibrium ablation Analysis of MUSES-C Super-Orbital Reentry Capsule," AIAA 1997-2481, *32nd AIAA Thermophysics Conference*, June 1997.

[5]Sharma, S. P., and Gillespie, W., Nonequilibrium and Equilibrium Shock Front Radiation Measurements, *Journal of Thermophysics and Heat Transfer*, Vol. 5, No. 3, 1991, pp. 257-265.

[6]Fujita, K., Sato, S., Abe, T., and Ebinuma, Y., Experimental Investigation of Air Radiation Behind a Strong Shock Wave, *Journal of Thermophysics and Heat Transfer*, Vol. 16, No. 1, 2002, pp. 77-82.

[7]Sakurai, K., Bindu, V. H., Niinomi, S., Ota, M., and Maeno, K., "CARS Measurement of Vibrational/Rotational Temperatures with Total Radiation Visualization behind Strong Shock waves of 5-7km/s," *27th International Symposium on*

Rarefied Gas Dynamics, AIP Conf. Proc. 1333, 2011, pp. 419-424.

[8]Kim, J. G. and Boyd, I. D., "State-resolved Master Equation Analysis of Thermochemical Nonequilibrium of Nitrogen," *Chemical Physics*, Vol. 415, 2013, pp. 237-246.

[9]Jaffe, R., Schwenke, D., Chaban, G., Huo, W., Vibrational and Rotational Excitation and Relaxation of Nitrogen from Accurate Theoretical Calculation, AIAA 2008-1208, *46th AIAA Aerospace Sciences Meeting and Exhibit*, Reno, Nevada, 2008.

[10]Jaffe, R., Schwenke, D., Chaban, G., Theoretical Analysis of N_2 Collisional Dissociation and Rotation-Vibration Energy Transfer, AIAA 2009-1569, *47th AIAA Aerospace Sciences Meeting and Exhibit*, Orlando, Florida, 2009.

[11]Parker, J. G., "Rotational and Vibrational Relaxation in Diatomic Gases," *Physics of Fluids*, Vol. 2, No. 4, 1959, pp. 449-462.

[12]Park, C., "Rotational Relaxation of N_2 Behind a Strong Shock Wave," *Journal of Thermophysics and Heat Transfer*, Vol. 18, No. 4, 2004, pp. 527-533.

[13]Hyun, S. Y., "Radiation Code SPRADIAN07 and Its Applications," Doctoral Thesis, KAIST, Daejeon, South Korea, 2009.

[14]Park, C., Jaffe, R., and Partridge, H., "Chemical-Kinetic Parameters of Hyperbolic Earth Entry," *Journal of Thermophysics and Heat Transfer*, Vol. 15, No. 1, 2001, pp. 76-90.

[15]Kim, J. G. and Boyd, I. D., "State-resolved thermochemical nonequilibrium analysis of hydrogen mixture flows," *Physcis of Fluids*, Vol. 24, No. 8, pp. 086102, 2012.

[16]Gnoffo, P. A., Gupta, R. N., and Shinn, J. L., "Conservation Equations and Physical Models for Hypersonic Air Flows in Thermal and Chemical Nonequilibrium," NASA TP-2867, Feb. 1989.

[17]Nishida, M., and Matsumoto, M., "Thermochemical Nonequilibrium in Rapidly Expanding Flows of High-Temperature Air," *Zeitschrift fur Naturforschung, Teil A. Physik, Physikalische Chemie, Kosmophysik*, Vol. 52, 1997, pp. 358-368.

[18]Millikan, R. C. and White, D. R., "Systematics of Vibrational Relaxation," *Journal of Chemical Physics*, Vol. 39, No. 12, 1963, pp. 3209-3213.

[19]Park, C., "Review o Chemical-Kinetic Problems of Future NASA Mission, I: Earth Entries," *Journal of Thermophysics and Heat Transfer*, Vol. 7, No. 3, 1993, pp. 385-398.

[20]Lee, J. H., "Electron-Impact Vibrational Relaxation in High-Temperature Nitrogen," *Journal of Thermophysics and Heat Transfer*, Vol. 7, No. , pp. 399-405.

[21]Bultel, A., Cheron, B., Boudon, A., Motapon, O., and Schneider, I., "Collisional-Radiative Model in Air for Earth Re-Entry Problems," Physics of Plasmas, Vol. 13, No. 4, 2006, pp. 1-11.

[22]Panesi, M., Magin, T, Bourdon, A., Bultel, A., and Chazot, O., "Fire II Flight Experiment Analysis by Means of a Collisional-Radiative Model," *Journal of Thermophysics and Heat Transfer*, Vol. 23, No. 2, 2009, pp. 236-248.

[23]Park, C., "Rate Parameters for Electronic Excitation of Diatomic Molecules I. Electron-Impact Processes," AIAA 2008-1206, *46th AIAA Aerospace Sciences Meeting and Exhibit*, Reno, Nevada, 2008.

[24]Park, C., "Rate Parameters for Electronic Excitation of Diatomic Molecules II. Heavy Particle-Impact Processes," AIAA 2008-1446, *46th AIAA Aerospace Sciences Meeting and Exhibit*, Reno, Nevada, 2008.

[25]Bourdon, A., and Vervisch, P., "Three Body Recombination Rates of Atomic Nitrogen in Low Pressure Plasma Flows," *Physical Review E*, Vol. 54, No. 2, 1996, pp. 1888-1898.

[26]Allen, R. A., "Nonequilibrium Shock Front Rotational, Vibrational, and Electronic Temperature Measurements," AVCO Everett Research Lab., Everett, MA, Research Rept. 186, Aug. 1964.

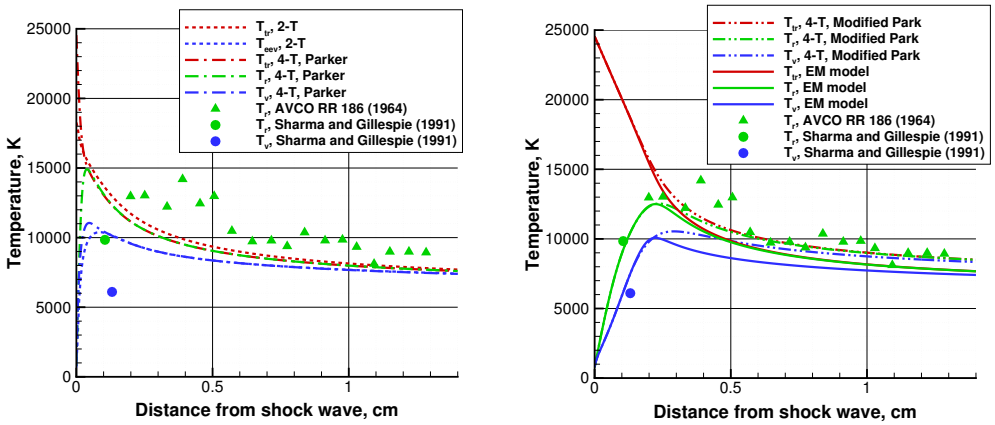

(a) 2-T and 4-T with Parker models

(b) 4-T with modified Park and EM models

Figure 1. Comparisons of the calculated translational, rotational, and vibrational temperatures with the shock-tube data measured by Sharma and Gillespie[5] and AVCO.[26]

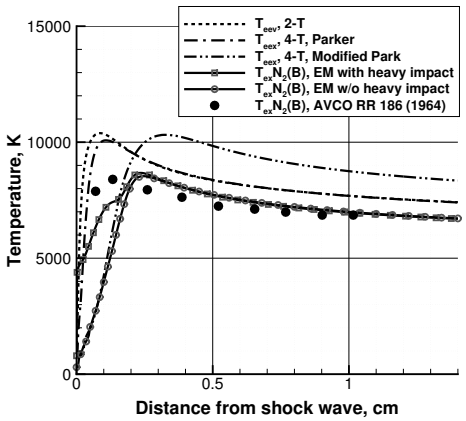

Figure 2. Comparisons of calculated electronic temperature of $N_2(B^3\Pi_g)$ with the shock-tube data measured by AVCO.[26]

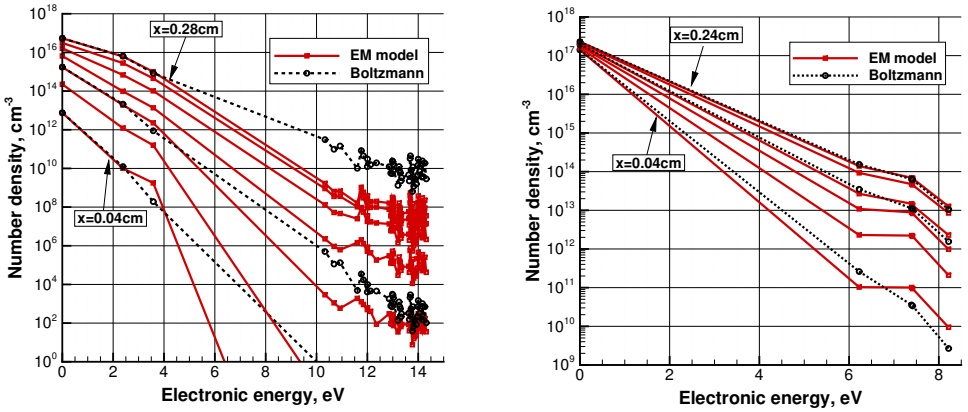

(a) Electronic number density populations of N (b) Electronic number density populations of N_2

Figure 3. Comparisons of the electronic number density populations of the EM model and the Boltzmann distributions specified by the electron temperature.

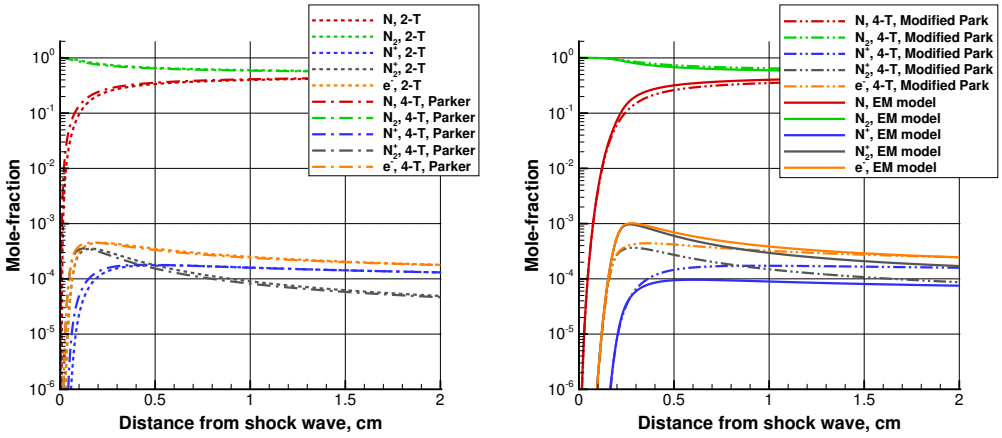

(a) 2-T and 4-T with Parker models (b) 4-T with modified Park and EM models

Figure 4. Comparisons of the species mole-fractions in the case of the shock-tube experiments by Sharma and Gillespie[5] and AVCO[26]

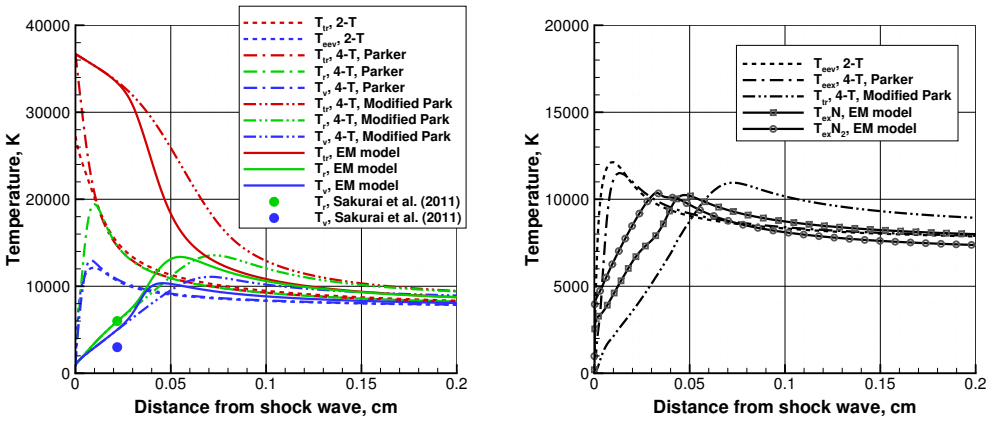

(a) 2-T and 4-T with Parker models (b) 4-T with modified Park and EM models

Figure 5. Comparisons of the calculated translational, rotational, and vibrational temperatures with the shock-tube data measured by Sakurai et al.[7]

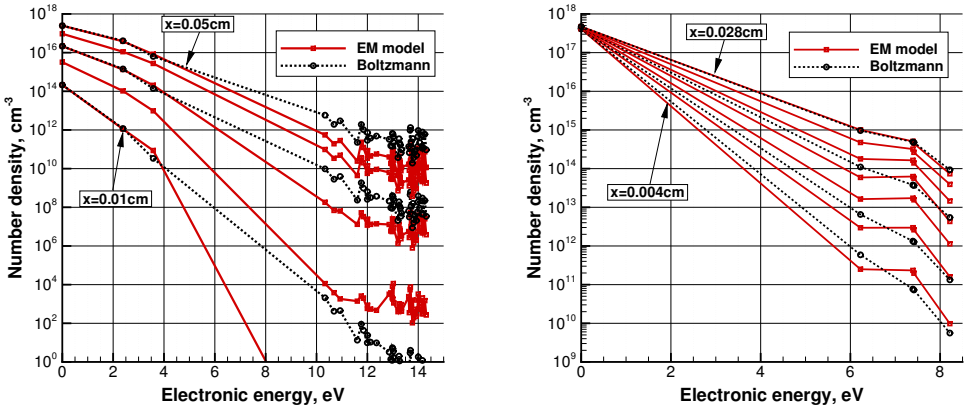

(a) N (b) N_2

Figure 6. Comparisons of the electronic number density populations of the EM model and the Boltzmann distributions specified by electron temperature

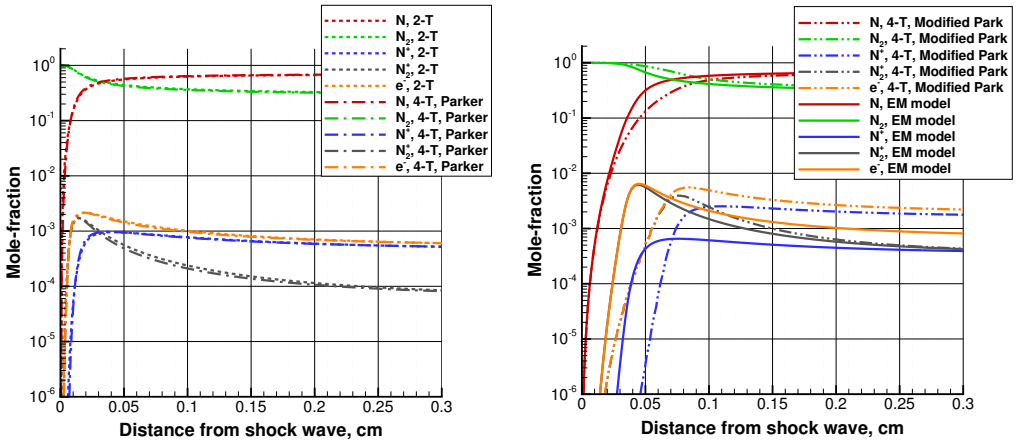

(a) 2-T and 4-T with Parker models

(b) 4-T with modified Park and EM models

Figure 7. Comparisons of the species mole-fractions in the case of the shock-tube experiments by Sakurai et al.[7]

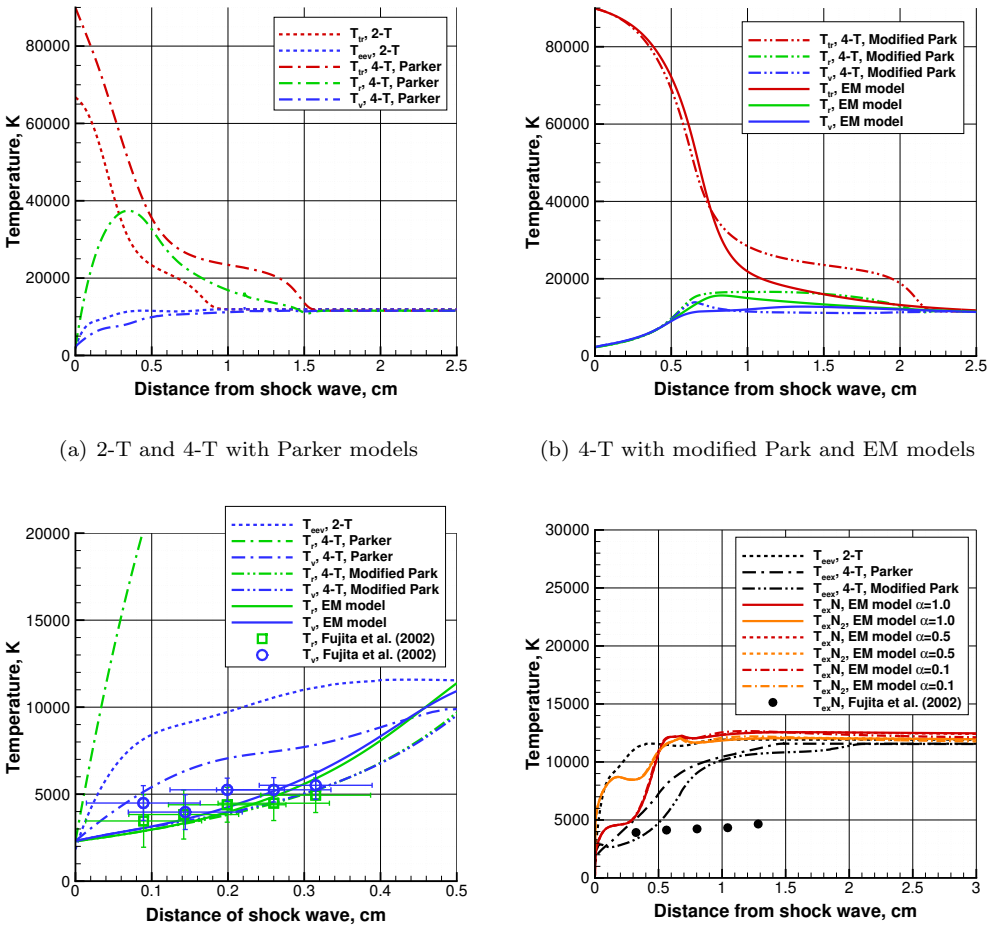

(a) 2-T and 4-T with Parker models

(b) 4-T with modified Park and EM models

(c) Comparisons of the rotational and vibrational temperatures

(d) Comparisons of the species electronic tempeatures

Figure 8. Comparisons of the calculated translational, rotational, vibrational, and electronic temperatures with the shock-tube data measured by Fujita et al.[6]

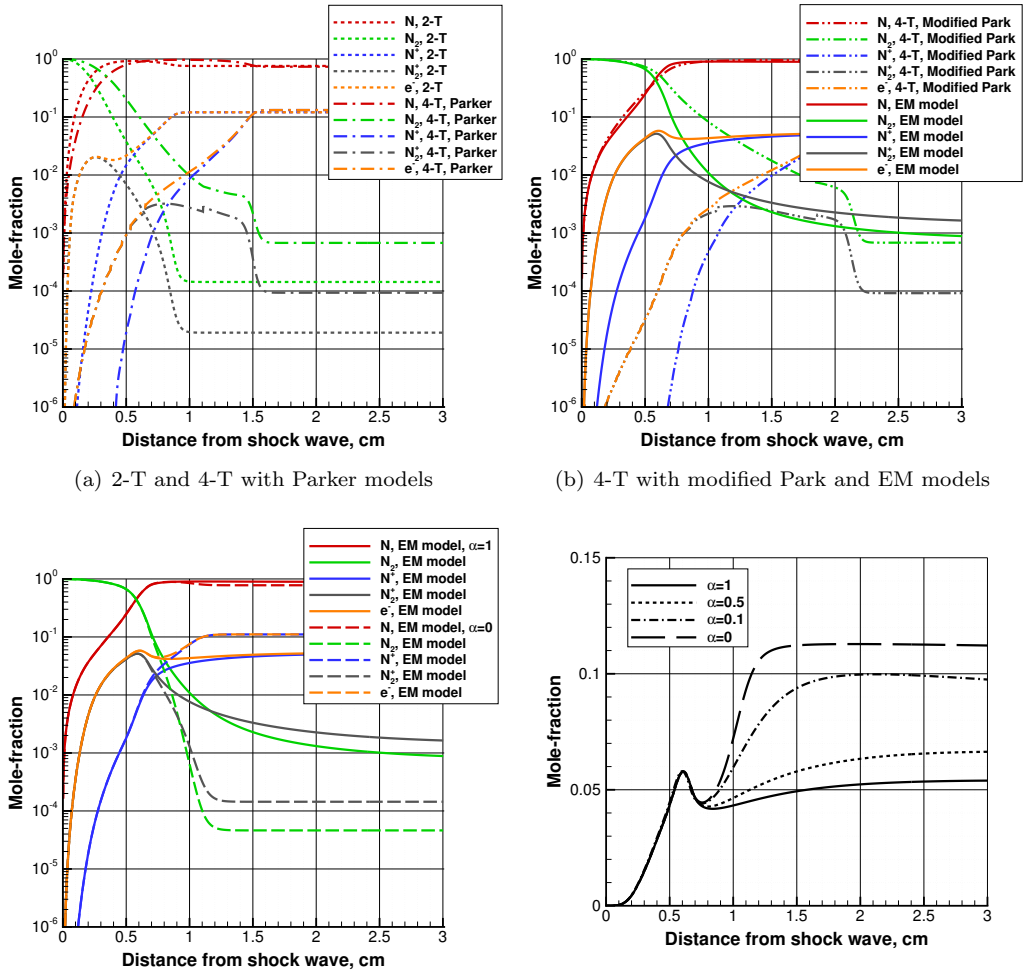

(a) 2-T and 4-T with Parker models

(b) 4-T with modified Park and EM models

(c) EM model with optically thin and thick mediums

(d) Electron number density

Figure 9. Comparisons of the species mole-fractions in the case of the shock-tube experiments by Fujita et al.[6]